iScience

Article

Nuclear transmembrane protein 199 promotes immune escapes by up-regulating programmed death ligand 1

Graphical abstract

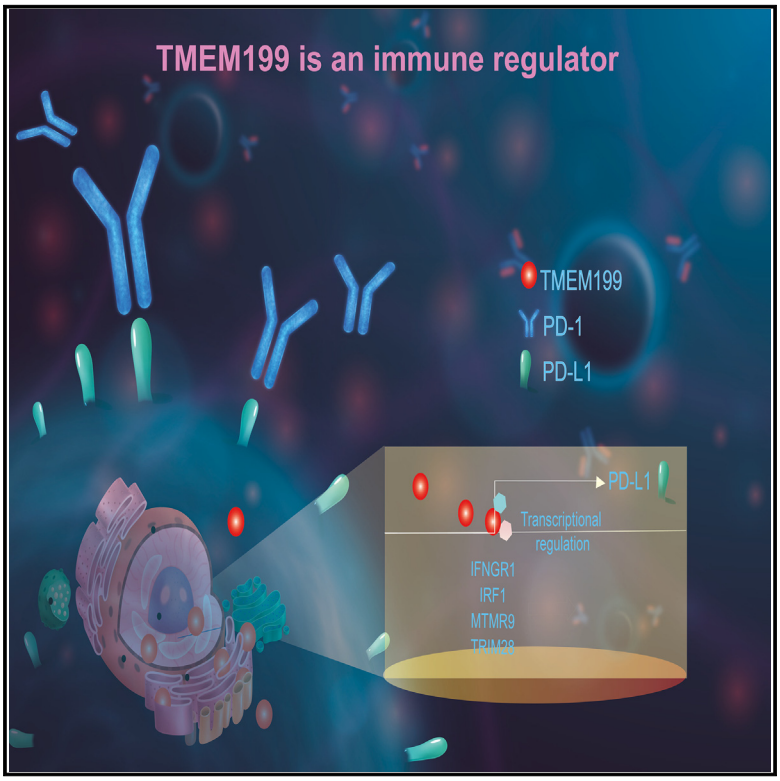

Authors

Wulin You, Hue Luu, Meili Li, ..., Mingsheng Cai, Tong-chuan He, Jingjing Li

Correspondence

tche@bsd.uchicago.edu (T.-c.H.), jingjingli.md.phd@gmail.com (J.L.)

In brief

Classification Description: Molecular biology; Molecular medicine

Highlights

- TMEM199 is located in the nuclear
- Nuclear TMEM199 regulates CD274 mRNA expression
- TMEM199 acts as a transcriptional co-factor
- TMEM199 modulates tumor microenvironment

You et al., 2024, iScience *27*, 111485
December 20, 2024
https://doi.org/10.1016/j.isci.2024.111485

CellPress

iScience

CellPress
OPEN ACCESS

Article

Nuclear transmembrane protein 199 promotes immune escapes by up-regulating programmed death ligand 1

Wulin You,[3,4,6] Hue Luu,[6] Meili Li,[5] Zhiyu Chen,[3,4] Fangchao Li,[1,2] Yanfei Zhang,[1,2] Mingsheng Cai,[5] Tong-chuan He,[6,*] and Jingjing Li[1,2,6,7,*]

[1]Affiliated Hospital, School of Clinical Medicine, Shandong Second Medical University, Weifang, Shandong, China
[2]Jinming Yu Academician Workstation of Oncology, Shandong Second Medical University, Weifang, Shandong, China
[3]Department of Orthopedics, Wuxi TCM Hospital Affiliated to Nanjing University of Chinese Medicine, Wuxi, Jiangsu Province, China
[4]Jiangsu CM Clinical Innovation Center of Degenerative Bone & Joint Disease, Wuxi TCM Hospital Affiliated to Nanjing University of Chinese Medicine, Wuxi, Jiangsu Province, China
[5]State Key Laboratory of Respiratory Disease, Guangdong Provincial Key Laboratory of Allergy & Clinical Immunology, Sino-French Hoffmann Institute, School of Basic Medical Science, Guangzhou Medical University, Guangzhou, China
[6]Molecular Oncology Laboratory, Department of Orthopedic Surgery and Rehabilitation Medicine, The University of Chicago Medical Center, Chicago, IL, USA
[7]Lead contact
*Correspondence: tche@bsd.uchicago.edu (T.-c.H.), jingjingli.md.phd@gmail.com (J.L.)
https://doi.org/10.1016/j.isci.2024.111485

SUMMARY

The function of transmembrane protein 199 (TMEM199) in cancer development has rarely been studied thus far. We report the nuclear localization of the TMEM199 protein and further analyzed the truncated fractions that mediate its nuclear localization. Cut&Tag assay globally explores the nuclear-located TMEM199 functions and tests its influence on the immune checkpoint PD-L1 *in vitro* and *in vivo*. Nuclear-located TMEM199 regulates PD-L1 mRNA levels by binding to transcription factors such as IFNGR1, IRF1, MTMR9, and Trim28, which all promote PD-L1 mRNA expression. Our study demonstrates the nuclear localization of TMEM199 and its immune regulation functions in cancer development. We uncovered the nuclear localization of TMEM199. TMEM199 is involved in CD274 mRNA gene expression by the transcriptional regulation of the upstream transcription factors or cofactors of CD274, such as IFNGR1, IRF1, MTMR9, KAT8, and Trim28. The nuclear-located TMEM199 is reported to address the tumor immune microenvironment commanding function.

INTRODUCTION

TMEM199 (transmembrane protein 199), also known as C17orf32, is recognized mostly because its mutations are associated with a rare genetic metabolic disease level called congenital disorder of glycosylation (CDG), which incites multisystemic manifestations including the developmental delay, developmental retardation, muscular hypotonus, nervous system disease, hepatopathy, and dysfunction of blood coagulation.[1–3] TMEM199 deficiency is also associated with fatty liver disease caused by impaired lysosomal function characterized by reduced acidification, autophagy, and increased lysosomal lipid accumulation.[4] TMEM199 also mediates the early stage of influenza A virus infection.[5]

However, the function of TMEM199 in cancer development has rarely been investigated until now. Bioinformatic analysis revealed that its high expression is significantly correlated with poor prognosis in hepatocellular carcinoma (HCC).[6]

TMEM199 is described as an accessory component of the critical proton pump for endolysosomal acidification, the proton-transporting vacuolar (V)-ATPase protein pump. TMEM199 involves activating Fe2+ prolyl hydroxylase (PHD) enzymes to maintain intracellular iron homeostasis.[7] TMEM199 is also involved in Golgi homeostasis. Its deficiency results in a hepatic phenotype with abnormal glycosylation.[8]

TMEM199 is a human homolog of yeast V-ATPase assembly factor Vph2p (also known as Vma12p). In yeast, V-ATPase assembly factors Vph2p, Vma21p, Pkr1p, and Vma22p are localized to the endoplasmic reticulum (ER).[9] Two labs have tried to demarcate the subcellular location of TMEM199. Jos C. Jansen declared that TMEM199 predominantly localizes to the ER-to-Golgi region, but not to the ER through a cellular compact marker protein colocalization analysis in 2016.[8] Subsequently, Anna L Miles et al. discloses that TMEM199 localizes to the ER which is required for endolysosomal acidification and lysosomal degradation.[7]

In this article, we report the nuclear localization of TMEM199 protein and further illustrate its function in mediating tumor immune microenvironment by regulating PD-L1 mRNA levels.

RESULTS

Transmembrane protein 199 displays nuclear localization

We noticed that TMEM199 amplification occurs in multiple cancer types (Figure 1A), including colon cancer, ovarian cancer, sarcoma et al. High TMEM199 expression contributed to worse

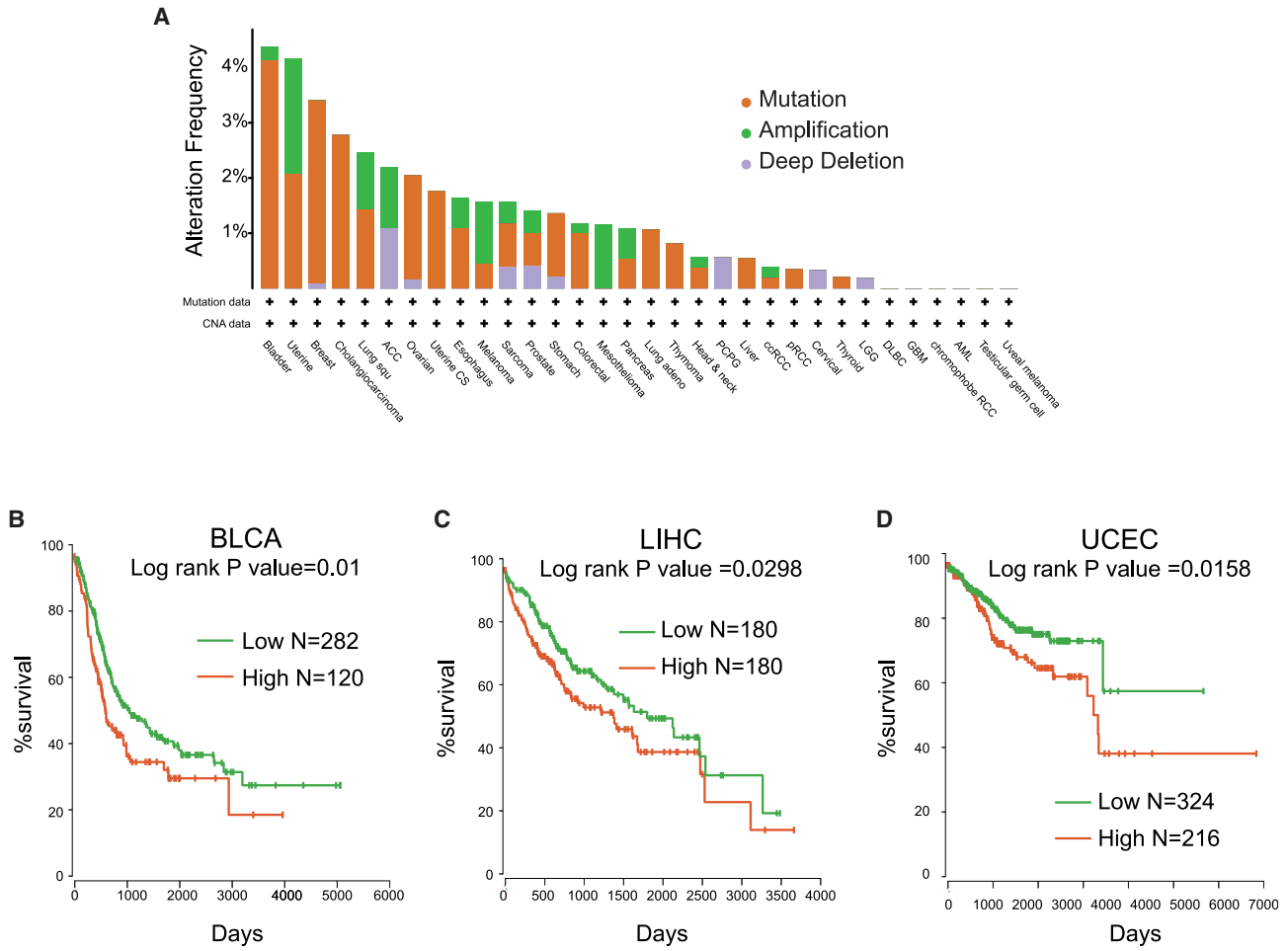

Figure 1. TMEM199 correlates to cancer prognosis

(A) Pan cancer analysis of the TMEM199 gene variation.

(B–D) Survival analysis of TMEM199 in different cancers.

survival in BLCA, LIHC, and UCEC (Figures 1B–1D). Therefore, TMEM199 potentially contributes to the cancer development process.

Jos C. Jansen reported that TMEM199 predominantly localizes to the endoplasmic reticulum (ER)-to-Golgi region, but not to the ER, through a cellular compact marker protein colocalization analysis in 2016.[8] Subsequently, Anna L Miles et al. revealed that TMEM199 localizes to the ER which is required for endolysosomal acidification and lysosomal degradation.[7] In our lab, to clarify the cellular localization of TMEM199, we performed co-immunoprecipitation coupled to mass spectrometry (co-IP/MS) assay.[10] We proposed to find the functional localization of TMEM199 by analyzing its interacting proteins. Then TMEM199 interacting proteins (TIPs) were pulled down with an anti-TMEM199 antibody and identified using mass spectrometry. Gene Ontology -Cellular Component (GOCC) analysis of TIPs revealed that TMEM199 is potentially functional at the cellular membrane, ribosome, extracellular component, and nucleus (Figure 2A). The nuclear interactors of TMEM199 imply the possibility of its novel functions. To confirm its nuclear localization, we designed different protocols in live or fixed cells. First, under conditions of paraformaldehyde (PFA) fixation and penetration with 0.025% Triton X-100, we found the nuclear localization of TMEM199 in multiple-originated cancer cells, human osteosarcoma cell 143B, colorectal carcinoma cell line HCT116 and ovarian cancer cell line Caov-3 (Figure 2B). Using three-dimensional (3D) reconstructions by confocal microscopy, the nuclear localization of TMEM199 was exhibited (Figure 2C). The above results are based on the localization of endogenous TMEM199. Additionally, Flag-tagged TMEM199 was present in the nuclear region (Figure 2D). Either PFA or Triton X-100 dissolves lipids of cellular membranes which interrupts the cell membrane integrity.[11–13] Considering the membrane localization property of TMEM199 as a transmembrane protein, we need to exclude the possibility of protein leakage from the cytoplasm to the nucleus caused by PFA and Triton X-100 induced membrane bursts. Therefore, we constructed a GFP-tagged TMEM199 expression plasmid and infected it into HEK293 cells. In living cells, we observed nuclear localization, although most of the proteins were still located in extranuclear regions (Figure 2E).

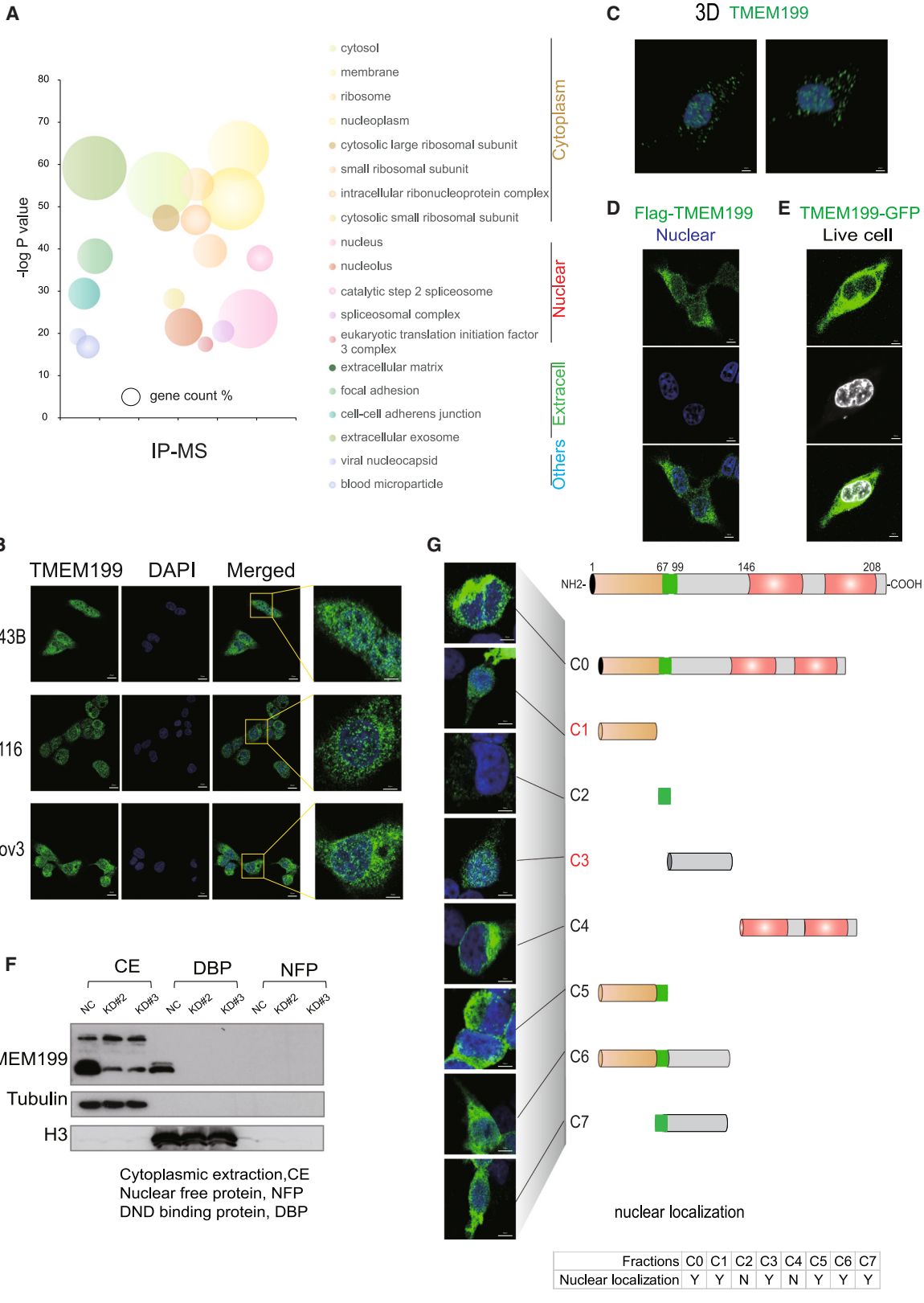

Fractions	C0	C1	C2	C3	C4	C5	C6	C7
Nuclear localization	Y	Y	N	Y	N	Y	Y	Y

(legend on next page)

For further verification, we extracted different cellular compact proteins and performed a Western blotting assay. The results suggest that the TMEM199 protein exists not only in the cytoplasmic fraction but also in the nuclear extraction (Figure 2F). These results suggest the nuclear localization of TMEM199.

Furthermore, we explored which fraction of TMEM199 leads to its nuclear localization. We did not find any classical nuclear localization signals (NLS) through TMEM199 protein sequence analysis. Then, we constructed Flag-tagged TMEM199 truncated fraction expressing vectors and transfected them into HEK293 cells, respectively. The fragments C1 and C3 localize in the nucleus (Figure 2G), which is consistent with the prediction of a non-canonical nuclear localization signal[14] (Figure S1A). Here, we report the nuclear location of TMEM199. However, regarding how the TMEM199 appears in the nuclear or translocates from the cytoplasm to the nucleus, it remains to be well clarified.

Nuclear transmembrane protein 199 function analysis points to the regulation of the immune response

Transcriptional regulation functions are common for nuclear proteins, including the direct DNA-bound proteins, transcriptional co-factors,[15] nuclear envelope proteins,[16–18] and also nucleolus proteins.[19] Thus, we proposed that TMEM199 potentially contributes to gene transcriptional regulation. For this purpose, we performed a Cut&Tag assay and global sequencing to disclose its gene binding profile. Binding peak analysis shows the binding sites (Figure 3A). To explore the genome-wide regulation of gene expression by TMEM199, we also measured the transcriptome alterations using RNA sequencing. Combining the Cut&Tag seq and RNA seq data, we estimated the regulatory potential by considering the bound peaks within 100 kb upstream and downstream of the transcription start site (TSS). A cumulative distribution[20] to determine the activating or repressive function of nuclear TMEM199 was depicted. Further activation/repression prediction showed that there was no inclination between its activation function and repression function (Figure 3C). Then, we performed *de novo* motif analysis which indicated the enriched transcription factor binding motifs of the forkhead box (FOX) protein members, such as *FoxM1*, *FoxI1*, *FoxK*, *Foxb1*, and *FoxL2* (Figure 3B). FOX transcription factors act on distinct molecular cascades regulating several biological processes such as metabolic reprogramming, inflammatory responses, aging, and autophagy et al.[21] FOX proteins engage in cancer initiation, progression, and also chemotherapeutic drug resistance in many cancers.[22–24] We analyzed the interacting nuclear proteins of TMEM199 from the nuclear extractions by IP–MS assay, which suggested that the FOX proteins above can interact with TMEM199(Table S2). One possibility can be inferred that TMEM199 attaches to the FOX protein and adheres to the gene binding site of the FOX proteins.

We performed bound gene functional analysis, which demonstrated that the TNF signaling pathway was significantly enriched (Figure S2A). Some immunoregulatory genes are bound by TMEM199, such as IFNGR1, IRF1, KAT8, c-Jun, and Trim28 (Figure 3D). IFNGR1 acts as a key factor in regulating demethylase JMJD2D-induced PD-L1 expression in colorectal cancer.[25] IRF1 responds to IFN-γ stimulation to modulate the cancer immune microenvironment.[26] Disrupting the phase separation of KAT8–IRF1 diminishes PD-L1 expression.[27] TRIM28 promotes the escape of gastric cancer cells from immune surveillance by increasing PD-L1 abundance.[28] We further performed a CHIP-qPCR assay to verify the gene promoter region binding (Figures 3E–3I). All of these cancer immune-associated genes are potentially regulated by nuclear TMEM199.

Perturbation of transmembrane protein 199 does not affect the growth of tumor cells themselves

We wondered whether TMEM199 contributes to cancer development. For this purpose, we constructed TMEM199 overexpression and knockdown plasmids. TMEM199-overexpressing or TMEM199-knockdown stable cell lines were established through lentivirus infection and antibiotic selection. Cell viabilities under TMEM199 overexpression or knockdown conditions were detected using the CCK8 kit. We have noticed that the cell growth was not influenced by TMEM199 disturbance (Figures 4A, S3A, and 6A). This conclusion was proved once more by the colony formation assay, which showed no differences in colony counts or sizes between TMEM199 knockdown and control cells (Figure 4C). Then we tested the cell invasion ability by Transwell migration assays and found that TMEM199 knockdown did not influence cell motility ability (Figure 4B). These results indicate that TMEM199 knockdown does not alter the cancer cell proliferation or invasion.

However, when we inoculated cancer cells with knocked TMEM199 stable cells into mice, the tumor sizes were significantly decreased (Figures 4D and 4E; Figure S3D). We propose that the immune environment *in vivo* context mediates this tumor reduction in TMEM199-depleted xenografts, whereas this effect cannot be reflected in the tumor cell-only environment *in vitro*. The infiltrated immune cells were analyzed, and the $CD8^+$ and CD11b+ cells were increased in the ratio in the TMEM199 knockdown xenografts, whereas the $CD4^+$ cells were decreased (Figures 4F–4H). RNA seq analysis demonstrated that the immune responses and tumor necrosis factor-mediated signaling

Figure 2. Nuclear localization of TMEM199

(A) Gene Ontology -Cellular Component (GOCC) analysis of TMEM199 interacted proteins (TIPs). TIPs are generated by co-IP/MS assay.

(B) Immunofluorescence assay to show nuclear localization in human osteosarcoma cell 143B, colorectal carcinoma cell line HCT116 as well as ovarian cancer cell line Caov-3, respectively. Photos are taken by confocal microscopy.

(C) 3D images of nuclear TMEM199, taken and reconstructed by Confocal Microscopy.

(D) Immunofluorescence assay to show the flag signal location when cells exogenously expressed TMEM-Flag protein.

(E) Live cell imaging to show the GFP signal in HEK293 cells with TMEM199-GFP plasmid transfection.

(F) Western blotting assay shows the cellular fracture TMEM199 containing content. CE, Cytoplasmic extraction; NFP, Nuclear free protein; DBP, DND binding protein.

(G) Immunofluorescence assay to show the cellular localized signals of truncated TMEM199 fractions.

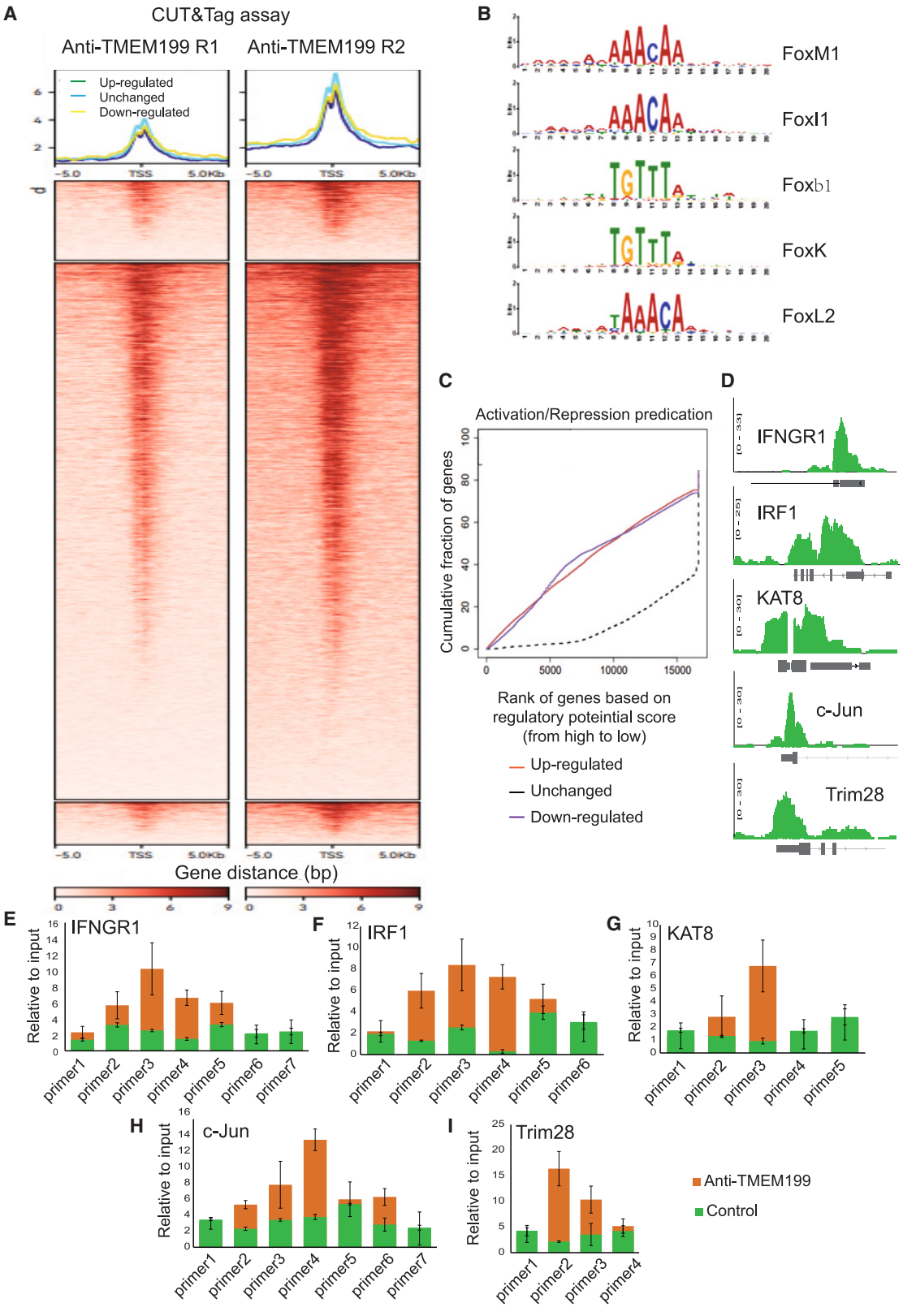

(legend on next page)

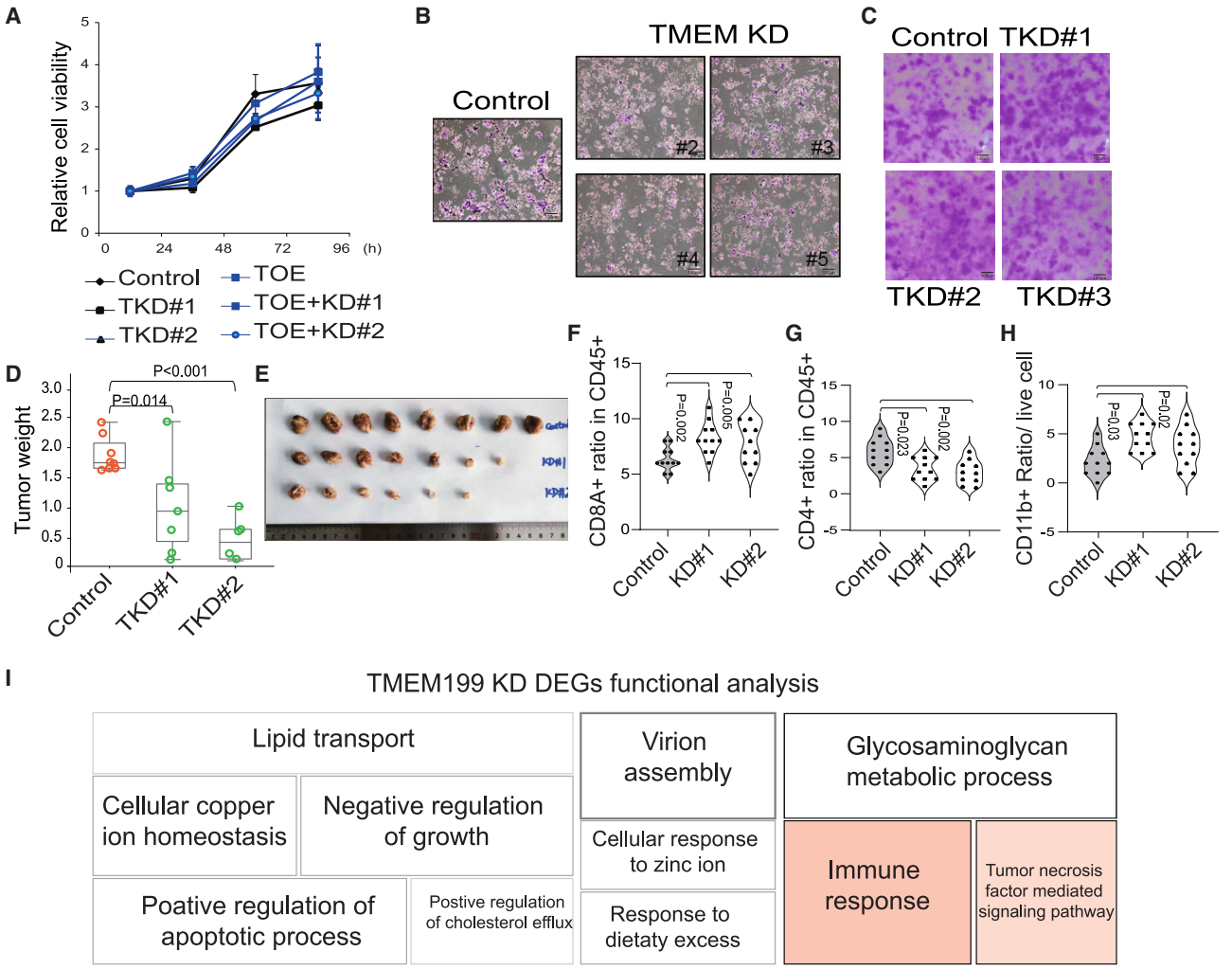

Figure 4. TMEM199 modulates Tumor microenvironment

(A) CCK8 assay to show the cell viabilities in 4T1 cells with TMEM199 knockdown or overexpression. KD means TMEM199 knock down; TOE means TMEM199 overexpression.

(B) Transwell assay to show the invasion abilities of 4T1 cells with TMEM199 knock down.

(C) Colony formation assay to show the cell proliferation ability in 4T1 cells with TMEM199 knock down.

(D and E) Tumor size analysis and Tumors imaging after the cells with TMEM199 knockdown xenograft in mice.

(F–H) Immune cell fractions analysis of the Tumor bulk.

(I) Gene ontology (GO) analysis of the enriched terms of differentially expressed genes (DEGs) in TMEM199 knock down versus control.

pathway gene ontology (GO) terms were enriched in the differentially expressed genes (DEGs) between control and TMEM199 knockdown cells (Figure 4I).

These results support that TMEM199 does not affect the cancer cell proliferation and invasion in a single tumor cell environment but has influences on the tumor immune microenvironment which consequently mediates the tumor bulk size.

Transmembrane protein 199 mediates the immune microenvironment

The *in vivo* assay results imply the potential role of TMEM199 in mediating the cancer microenvironment; thus, we further analyzed the expression of TMEM199 and its correlation with immune infiltration across cancers. The correlation of TMEM199 and immune cells was mapped and showed that TMEM199 is

Figure 3. Functional analysis of the nuclear TMEM199

(A) Heatmaps describing TMEM199 Cut&Tag enrichment at peaks. R1 and R2 are two independent Cut&Tag tests with different sequencing depth.

(B) Logo representation of the motif found to be enriched in the TMEM199 Cut&Tag.

(C) Activation and repression correlation analysis of TMEM199 bound genes combined with the RNA sequencing data.

(D) Presentive binding peaks of TMEM199 according to the Cut&Tag assay.

(E–I) CHIP-qPCR detects the enriched binding of transcriptional factors at CD274 TSS. Data are represented as mean ± SEM.

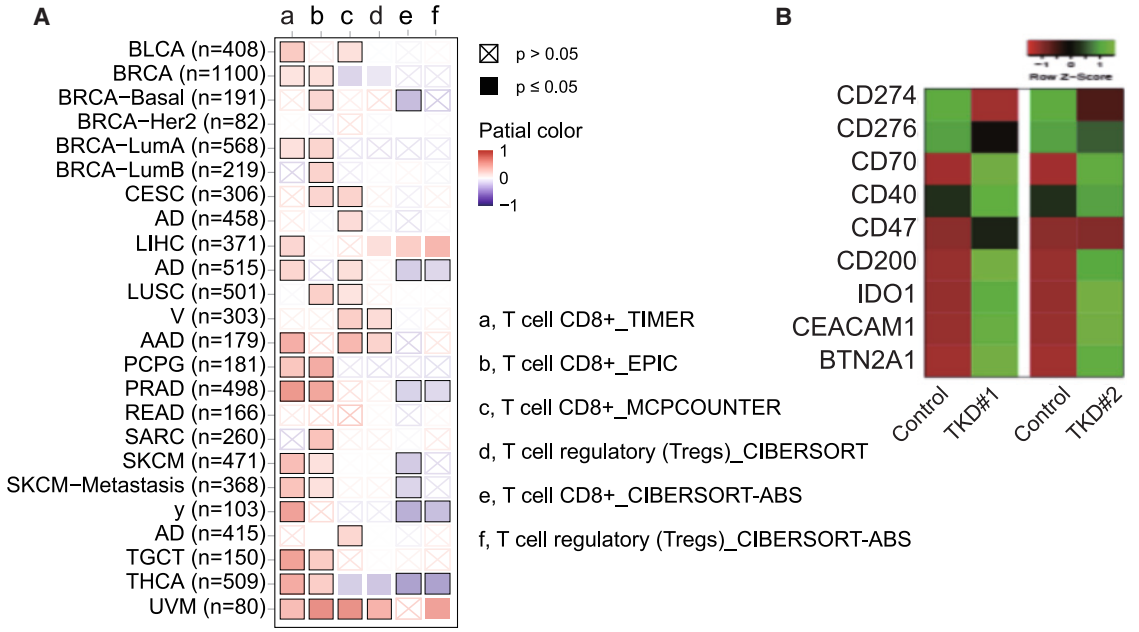

Figure 5. Pan-cancer analysis shows TMEM199 correlates to immune responses

(A) Pan cancer analysis of the correlation between TMEM199 expression level and infiltrating immune cells.

(B) Heatmap to show the immune check points alteration in TMEM199 knocked down cells.

correlated with cancer immune infiltration (Figure 5A). Then, immune checkpoints are detected in TMEM199-knock cells, which show an alternative profile of immune escape. CD274 and CD276 expression levels were reduced in TMEM199 knockout cells; in contrast, CD70, IDO1, BTN2A1, and other immune checkpoints were upregulated (Figure 5B). This evidence supports that TMEM199 works as a baton of immune microenvironment regulation.

Transmembrane protein 199 conducts CD274 mRNA expression

CD274, also commonly referred to as programmed death ligand 1 (PD-L1) is an essential immune checkpoint protein. Cancer cell PD-L1 interacts with programmed death 1 (PD-1) on T lymphocytes which exerts adaptive immune escape by inducing tumor-infiltrating T cell apoptosis by restraining T cell activation, proliferation, cell survival, and effector functions.[29–31] Here, we have observed that TMEM199 knockdown decreased CD274 levels (Figure 5B). Consistently, in TMEM199 knockdown cells, the PD-L1 protein level was decreased, which was validated with multiple different cancer cells (Figures 6A–6D). Flow cytometry (FCM) analysis also showed a decreased signal intensity of PD-L1 in the cell membrane (Figure 6F). When TMEM199 was reversed, the PD-L1 level also is recovered (Figure 6E).

Combined with the results of the Cut&Tag assay, we proposed that TMEM199 regulates PD-L1 expression by mediating transcription factors such as IFNGR1, IRF1, c-Jun, KAT8, and Trim28. To substantiate this hypothesis, the knockdown plasmids were used to target the transcription factors IFNGR1. IRF1, c-Jun, and Trim28 were constructed and packaged in a lentivirus system. Transient infection to cancer cells was performed for the knockdown effect validation (Figures S4A–S4E). Having confirmed that the plasmids work well, we tested whether the transcription factors mentioned above affect CD274 mRNA expression levels. For instance, when TMEM199 was knocked down, a significant decrease in the CD274 mRNA expression level was observed. In contrast, when we overexpressed Flag-tagged TMEM199, the CD274 mRNA expression level was reversed. In a uniform cell background in which the knockdown cells were all compensated with overexpressed TMEM199, IGNR1 knockdown decreased CD274 mRNA levels (Figure 7J). The same trends were also observed in cells with IRF1, c-Jun, KAT8, or Trim28 knockdown (Figures 7H, S4F–S4H). These results suggest that transcription factors or cofactors such as IFNGR1, IRF1, c-Jun, KAT8, and Trim28 might interact with TMEM199 to regulate CD274 mRNA expression.

Transmembrane protein 199 does not influence programmed death ligand 1 protein degradation

Considering the possibility that TMEM199 may influence its protein degradation sector, the vast majority of TMEM199 protein localizes in cytoplasmic organelles. Cycloheximide (CHX) is added to cultured cells to block the newly transcribed messages.[32] Then, we tested the cell membrane PD-L1 signal intensity in TMEM199 knockout stable cells. In response to stimulation by IFNγ, there was no significant difference between TMEM199 knockout cells and control cells (Figure 7A). This indicates that TMEM199 knockout does not impact the PD-L1 degradation. This can be verified again through the immunofluorescence assay. In the stable TMEM199 knockout cells, the TMEM199 and endogenous PD-L1 proteins were both

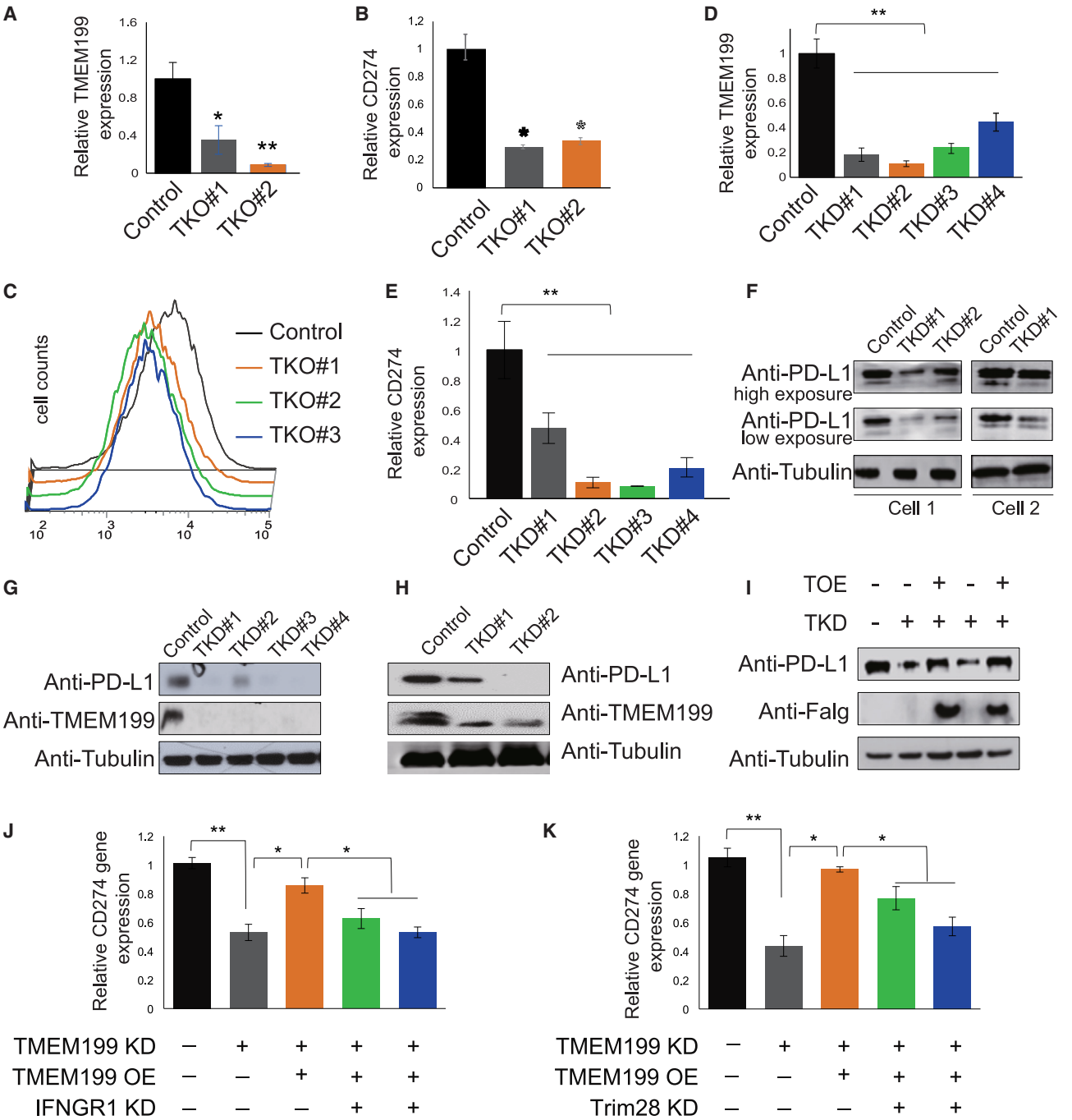

Figure 6. TMEM199 regulate PD-L1 mRNA level

(A) Relative TMEM199 expression level in TMEM199 knock out cells with different oligos (*, $p < 0.05$; **, $p < 0.01$; ***, $p < 0.001$). Data are represented as mean ± SEM.

(B) Relative CD274 mRNA level in TMEM199 knock out cells with different oligos (*, $p < 0.05$; **, $p < 0.01$; ***, $p < 0.001$). Data are represented as mean ± SEM.

(C) Flow Cytometry (FCM) analysis to show the PD-L1 fluorescence intensity in the cytoplasmic membrane when TMEM199 was knocked out. TKO, TMEM199 knock out; #1, #2, #3, TMEM199 was knocked out with different oligos.

(D) Relative TMEM199 mRNA expression level when TMEM199 was knocked down (*, $p < 0.05$; **, $p < 0.01$; ***, $p < 0.001$).

(E) Relative CD274 mRNA expression level when TMEM199 was knocked down (*, $p < 0.05$; **, $p < 0.01$; ***, $p < 0.001$). Data are represented as mean ± SEM.

(F–H) Western blotting to show the TMEM199 protein level and PD-L1 protein level under TMEM199 knockdown conditions. For (F), cell1 is HCT116 cells, cell2 is 143B cells; For (G), it is done in 4T1 cells; (H) is done in CaoV-3 cells.

(I) Western blotting assay shows the PD-L1 protein level when TMEM199 was compensated to cells with TMEM199 knockdown.

(J and K) QPCR shows the CD274 mRNA level when IFNGR1 (J) or Trim28 (K) was depressed (*, $p < 0.05$; **, $p < 0.01$; ***, $p < 0.001$). Data are represented as mean ± SEM.

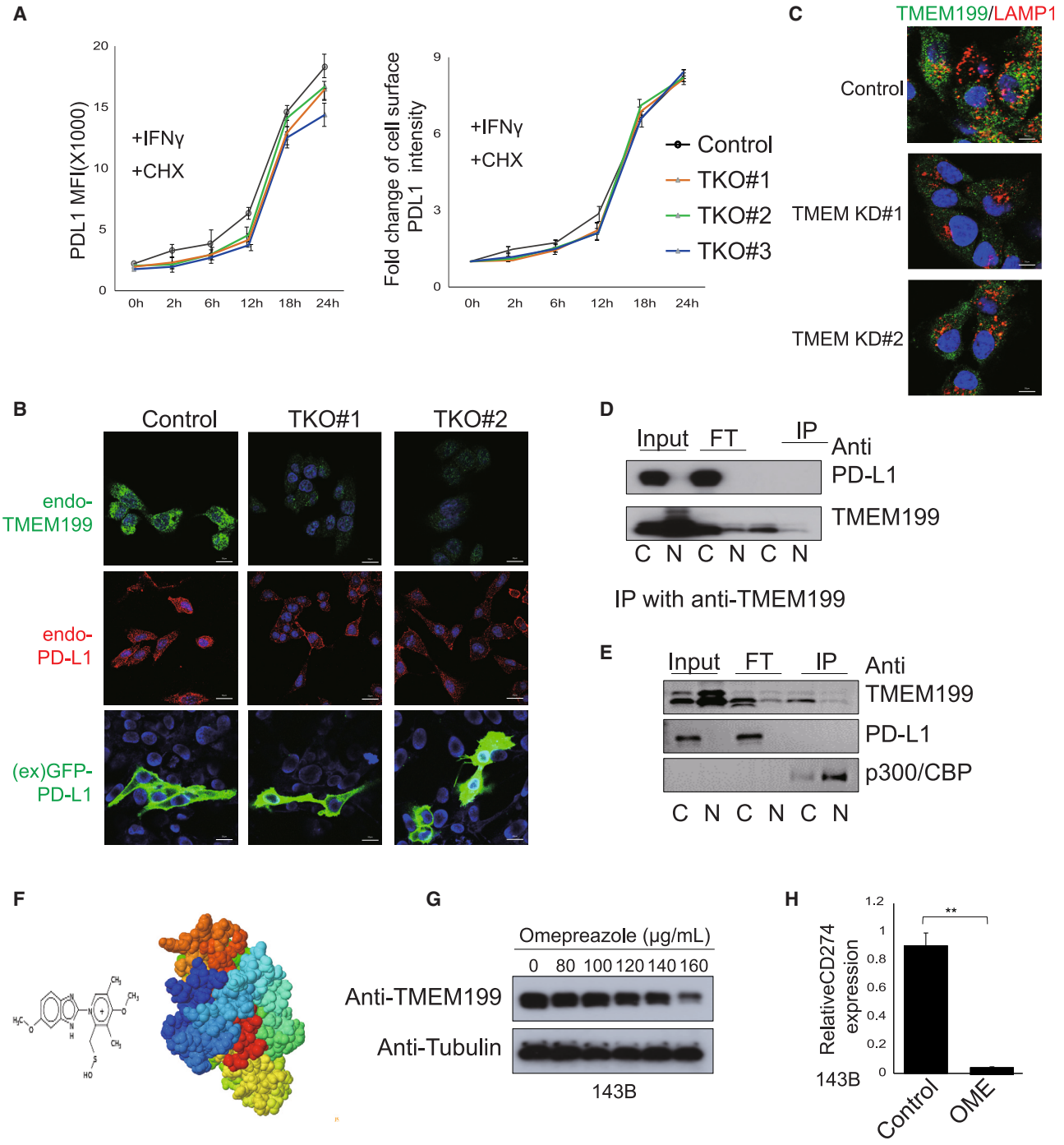

Figure 7. Effect of TMEM199 on PD-L1 degradation

(A) Mean fluorescence intensity in cytoplasmic membrane when TMEM199 was knocked out. All cells are treated with equal dose of IFNgama and Cycloheximide (CHX), an inhibitor of eukaryotic translation.

(B) Immunofluorescence assay to show the TMEM199, endogenous PD-L1 as well as exogenous PD-L1 protein level when TMEM199 was knocked down in 143B cells.

(C) Immunofluorescence assay to show TMEM199 and LAMP1 staining signals when TMEM199 was knocked down (KD#1 and KD#2 are different oligoes).

(D and E) Western blotting following the co-immunoprecipitation to display the potential TMEM199-PD-L1 protein-protein interaction.

(F) Skeletal formula of Omeprezole and predicted TMEM199 3D structure.

(G) TMEM199 protein level when cells are treated with Omeprezole.

(H) CD274 mRNA level when cells are treated with Omeprezole.

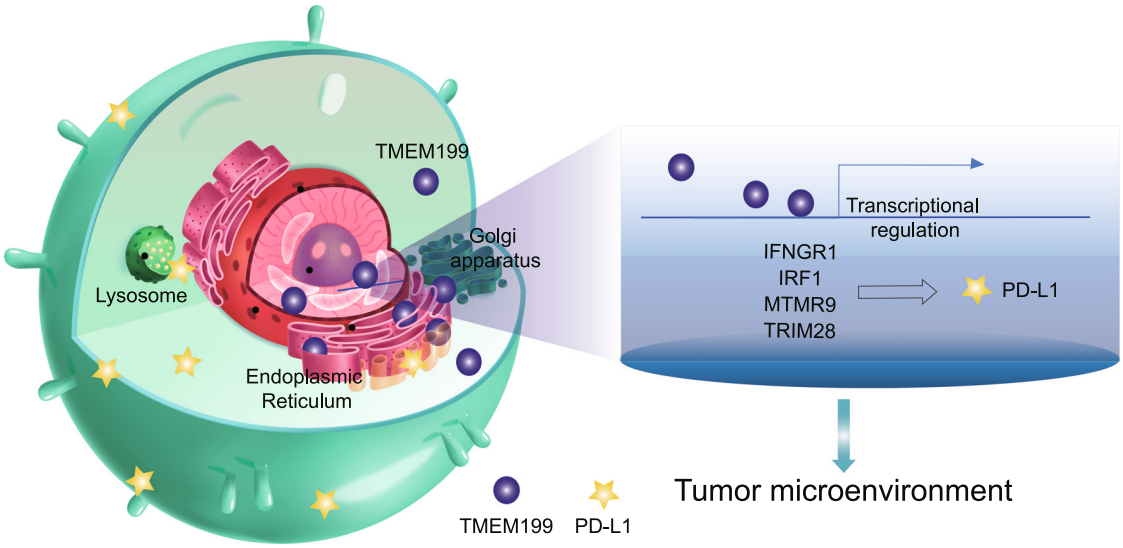

Figure 8. Mechanism diagram of nuclear TMEM199 regulating PD-L1

Diagram to show the cellular localization of TMEM199 and its function in transcriptional regulation IFNGR1, IRF1, MTMR9, and Trim28, which further control PD-L1 mRNA level.

exhausted; however, the exogenous PD-L1 protein obtained by transfection was not discounted due to TMEM199 knockout (Figures 7B and S5A). In contrast, when the translation was inhibited by CHX, the exogenous PD-L1 protein level was upregulated (Figure S5C).

In addition, we detected the lysosome biogenesis in TMEM199 knockdown cells. In contrast to a previous report that insists that loss of TMEM199 results in compensatory lysosomal adaptation and biogenesis after V-type ATPase inactivation,[33] a significantly decreased lysosome quantity was exposed (Figures 7C and S5B). Increasing evidence shows that lysosomes are one of the essential degradation paths for PD-L1 protein.[34,35] Lysosome deficiency caused by TMEM199 knockdown might impair protein degradation. This explains why TMEM199 knockdown increased PD-L1 protein expression in the context of translational inhibition (Figure S5C). In addition, we also tested EGFR and HLA protein levels in TMEM199 knockout cells under a translation inhibition background. Both EGFR and HLA can be degraded through lysosomes, although this is not the only path[36–38] (Figures S5E). As we expected, both EGFR and HLA protein levels were enhanced due to TMEM199 knockout (Figure S5D). Moreover, we excluded the possibility of a direct interaction between TMEM199 and PD-L1 (Figures 7D and 7E).

We also found that the proton pump inhibitor (PPI) omeprazole significantly decreased TMEM199 protein levels (Figure 7H and S6A). Correspondingly, CD274 mRNA was largely decreased by omeprazole (Figures 7I and S6B). This suggests that TMEM199 is a targetable immune regulator.

Conclusion

We proved the nuclear localization of TMEM199. Our new foundings also imply that TMEM199 is involved in CD274 mRNA gene expression by the transcriptional regulation of the upstream transcription factors or cofactors of CD274, such as IFNGR1, IRF1, MTMR9, KAT8, and Trim28 (Figure 8).

DISCUSSION

Approximately 5000∼6000 alpha-helical transmembrane protein-coding genes in *Homo sapiens,* and 27% of the total human proteome are alpha-helical transmembrane proteins.[39,40] Transmembrane proteins participate in various vital biological processes such as signal transduction, transportation, membrane trafficking, and immune responses.[41–43] Roughly 10% of eukaryotic transmembrane proteins localize to the nuclear membrane, although the mechanisms by which transmembrane proteins directly traffic or translocate to the nucleus remain in dispute.[44] Mounting evidence suggests that proteins are originally to be recognized as localized only on the plasma membrane may localize to the nucleus.[45–48] Transmembrane proteins with multiple transmembrane domains are rarely found in nuclear localization. However, recently, Hongxia Wang's lab recently reported the nuclear translocation of the 4-pass transmembrane protein Tspan8 by using the machinery for the nuclear translocation of cytosolic proteins.[49]

In this research, we proposed that the functional localization of TMEM199 can be directed by analyzing its interacting proteins. Therefore, we performed a co-IP/MS assay. TIP cellular component enrichment analysis led us to consider the potentiality of TMEM199 nuclear localization. Using different experimental methods, either in fixed cells or in live cells, the nuclear localization of TMEM199 was finally verified. However, we did not conduct in-depth research regarding how TMEM199 translocates into the nucleus or directly targets it. The mechanism of its nuclear targeting is worthy of attention. The majority of TMEM199 is expressed in the cytoplasm. However, we did not find TMEM199 interacted with PD-L1 protein (Figures 7D and

7E). Meanwhile, we noticed the nuclear localization of TMEM199 and CD274 mRNA alteration caused by TMEM199 overexpression or knock down. Thus, we emphasize the nuclear TMEM199 function in regulating PD-L1. However, the cytoplasmic function cannot be ignored in other functions of TMEM199.

Through the analysis of high-throughput sequencing data, TMEM199 is implied to be functional in cancer immune responses. Unexpectedly, TMEM199 knockdown or expression did not impact cancer cell proliferation and invasion. However, once cells were in the context of the immune microenvironment, tumors with TMEM199 knockdown notably diminished.

A Cut&Tag assay was performed to globally analyze TMEM199-bound gene sites. TMEM199 binds to the gene promoter sites of IFNGR1, IRF1, MTMR9, KAT8, and Trim28, which are all regulatory factors of PD-L1, to induce immune escape. PD-L1 expression is widely regulated by transcriptional or co-transcriptional factors, such as Myc, BRD4, STATs, NFkB, and so on.[50] Besides, epigenetic regulation is also essential for modulating PD-L1 expression.[50] Here, we reported TMEM199 as a novel co-transcriptional factor to regulate PD-L1. It is reasonable that we observed that TMEM199 does not affect cancer cell proliferation and invasion in a single tumor cell environment but influences the tumor immune microenvironment, which consequently mediates tumor bulk size.

Finally, we found that TMEM199 can be targeted by the proton pump inhibitor (PPI) omeprazole. PPI application disrupts immune therapy in the clinic and is attracting increasing attention.[51] The concurrent work of our lab is to illustrate the role of TMEM199 in influencing PPI immunotherapy and then seek a replacement drug for the patients who accept immunotherapy and chemotherapy.

Limitations of the study

We found the nuclear localization of TMEM199. However, the majority of TMEM199 spreads in the cytoplasmic region. How this transmembrane protein enters the nuclear remains unstated in this article.

Besides, the mechanism of how the PPI decreases TMEM199 protein level is still unintelligible. Further exploration should focus on this point.

RESOURCE AVAILABILITY

Lead contact

Further information and requests for resources should be directed to and will be fulfilled by the lead contact, Jingjing Li (jingjinglimdphd@uchicago.edu).

Materials availability

This study did not generate new unique reagents.

Data and code availability

- All data reported in this article will be shared by the lead contact upon request.
- This article does not report the original code.
- Any additional information required to reanalyze the data reported in this article is available from the lead contact upon request.

ACKNOWLEDGMENTS

In this work Jingjing Li is supported by the National Natural Science Foundation of China (Grant No. 82104289), Shandong Provincial Health Commission (M-2022053), Science and Technology Innovation Plan from Weifang Medical University (041004), Yuandu Scholar Grant of Weifang City to LJJ, Weifang Science and Technology Bureau Plan Project (2021YX081), Science and technology project jointly established by the Science and Technology Department of the State Administration of Traditional Chinese Medicine (GZY-KJS-SD-2023-079), Shandong Provincial Medical Association Young Talent Promotion Project (2023_GJ_0039). Science and Technology Innovation Plan from Weifang Medical University (041011). Wulin You is supported by Top Talent Support Program for young and middle-aged people of Wuxi Health Committee (Grant No. BJ2023070).

AUTHOR CONTRIBUTIONS

Jingjing Li and Tongchuan He designed the research; Jingjing Li, Wulin You, Meili Li, Zhiyu Chen, Fangchao Li, and Yanfei Zhang performed the experiments. Jingjing LI, Wulin You, and Tong-chuan He wrote and organized the article; Tong-chuan He,Mingsheng Cai, and Hue Luu revised the article and reorganized the figures.

DECLARATION OF INTERESTS

The authors declare that they have no competing interests.

STAR★METHODS

Detailed methods are provided in the online version of this paper and include the following:

- KEY RESOURCES TABLE
- EXPERIMENTAL MODEL AND STUDY PARTICIPANT DETAILS
  - Cells
  - Mice
- METHOD DETAILS
  - Cell lines, chemicals and antibodies
  - CCK8 assay
  - Transwell migration assay
  - Co-IP assay
  - Protein identification by MS and bioinformatic analysis
  - Colony formation assay
  - Immunofluorescence assay
  - Western blotting
  - Transcriptome analysis
  - Cut&Tag assay
  - Animal experiment
- QUANTIFICATION AND STATISTICAL ANALYSIS

SUPPLEMENTAL INFORMATION

Supplemental information can be found online at https://doi.org/10.1016/j.isci.2024.111485.

Received: June 25, 2024
Revised: October 5, 2024
Accepted: November 25, 2024
Published: November 28, 2024

REFERENCES

1. Fang, Y., Abuduxikuer, K., Wang, Y.Z., Li, S.M., Chen, L., and Wang, J.S. (2022). TMEM199-Congenital Disorder of Glycosylation With Novel Phenotype and Genotype in a Chinese Boy. Front. Genet. *13*, 833495. https://doi.org/10.3389/fgene.2022.833495.

2. Vajro, P., Zielinska, K., Ng, B.G., Maccarana, M., Bengtson, P., Poeta, M., Mandato, C., D'Acunto, E., Freeze, H.H., and Eklund, E.A. (2018). Three unreported cases of TMEM199-CDG, a rare genetic liver disease with abnormal glycosylation. Orphanet J. Rare Dis. *13*, 4. https://doi.org/10.1186/s13023-017-0757-3.

3. Fiumara, A., Sapuppo, A., Ferri, L., Arena, A., Prato, A., Garozzo, D., Sturiale, L., Morrone, A., and Barone, R. (2023). Higher frequency of TMEM199-CDG in the southern mediterranean area is associated with c.92G>C (p.Arg31Pro) mutation. Eur. J. Med. Genet. *66*, 104709. https://doi.org/10.1016/j.ejmg.2023.104709.

4. Larsen, L.E., van den Boogert, M.A.W., Rios-Ocampo, W.A., Jansen, J.C., Conlon, D., Chong, P.L.E., Levels, J.H.M., Eilers, R.E., Sachdev, V.V., Zelcer, N., et al. (2022). Defective Lipid Droplet-Lysosome Interaction Causes Fatty Liver Disease as Evidenced by Human Mutations in TMEM199 and CCDC115. Cell. Mol. Gastroenterol. Hepatol. *13*, 583–597. https://doi.org/10.1016/j.jcmgh.2021.09.013.

5. Li, B., Clohisey, S.M., Chia, B.S., Wang, B., Cui, A., Eisenhaure, T., Schweitzer, L.D., Hoover, P., Parkinson, N.J., Nachshon, A., et al. (2020). Genome-wide CRISPR screen identifies host dependency factors for influenza A virus infection. Nat. Commun. *11*, 164. https://doi.org/10.1038/s41467-019-13965-x.

6. Zhao, X., Chen, J., Yin, S., Shi, J., Zheng, M., He, C., Meng, H., Han, Y., Han, J., Guo, J., et al. (2022). The expression of cuproptosis-related genes in hepatocellular carcinoma and their relationships with prognosis. Front. Oncol. *12*, 992468. https://doi.org/10.3389/fonc.2022.992468.

7. Miles, A.L., Burr, S.P., Grice, G.L., and Nathan, J.A. (2017). The vacuolar-ATPase complex and assembly factors, TMEM199 and CCDC115, control HIF1alpha prolyl hydroxylation by regulating cellular iron levels. Elife *6*, e22693. https://doi.org/10.7554/eLife.22693.

8. Jansen, J.C., Timal, S., van Scherpenzeel, M., Michelakakis, H., Vicogne, D., Ashikov, A., Moraitou, M., Hoischen, A., Huijben, K., Steenbergen, G., et al. (2016). TMEM199 Deficiency Is a Disorder of Golgi Homeostasis Characterized by Elevated Aminotransferases, Alkaline Phosphatase, and Cholesterol and Abnormal Glycosylation. Am. J. Hum. Genet. *98*, 322–330. https://doi.org/10.1016/j.ajhg.2015.12.011.

9. Forgac, M. (2007). Vacuolar ATPases: rotary proton pumps in physiology and pathophysiology. Nat. Rev. Mol. Cell. Biol. *8*, 917–929. https://doi.org/10.1038/nrm2272.

10. Richards, A.L., Eckhardt, M., and Krogan, N.J. (2021). Mass spectrometry-based protein-protein interaction networks for the study of human diseases. Mol. Syst. Biol. *17*, e8792. https://doi.org/10.15252/msb.20188792.

11. Fox, C.H., Johnson, F.B., Whiting, J., and Roller, P.P. (1985). Formaldehyde fixation. J. Histochem. Cytochem. *33*, 845–853. https://doi.org/10.1177/33.8.3894502.

12. Thavarajah, R., Mudimbaimannar, V.K., Elizabeth, J., Rao, U.K., and Ranganathan, K. (2012). Chemical and physical basics of routine formaldehyde fixation. J. Oral Maxillofac. Pathol. *16*, 400–405. https://doi.org/10.4103/0973-029X.102496.

13. Cheng, R., Zhang, F., Li, M., Wo, X., Su, Y.W., and Wang, W. (2019). Influence of Fixation and Permeabilization on the Mass Density of Single Cells: A Surface Plasmon Resonance Imaging Study. Front. Chem. *7*, 588. https://doi.org/10.3389/fchem.2019.00588.

14. Nguyen Ba, A.N., Pogoutse, A., Provart, N., and Moses, A.M. (2009). NLStradamus: a simple Hidden Markov Model for nuclear localization signal prediction. BMC. Bioinf. *10*, 202. https://doi.org/10.1186/1471-2105-10-202.

15. Haberle, V., Arnold, C.D., Pagani, M., Rath, M., Schernhuber, K., and Stark, A. (2019). Transcriptional cofactors display specificity for distinct types of core promoters. Nature *570*, 122–126. https://doi.org/10.1038/s41586-019-1210-7.

16. Somech, R., Shaklai, S., Geller, O., Amariglio, N., Simon, A.J., Rechavi, G., and Gal-Yam, E.N. (2005). The nuclear-envelope protein and transcriptional repressor LAP2beta interacts with HDAC3 at the nuclear periphery, and induces histone H4 deacetylation. J. Cell. Sci. *118*, 4017–4025. https://doi.org/10.1242/jcs.02521.

17. Schirmer, E.C., Florens, L., Guan, T., Yates, J.R., 3rd, and Gerace, L. (2003). Nuclear membrane proteins with potential disease links found by subtractive proteomics. Science *301*, 1380–1382. https://doi.org/10.1126/science.1088176.

18. Brown, C.R., and Silver, P.A. (2007). Transcriptional regulation at the nuclear pore complex. Curr. Opin. Genet. Dev. *17*, 100–106. https://doi.org/10.1016/j.gde.2007.02.005.

19. Antoniali, G., Lirussi, L., Poletto, M., and Tell, G. (2014). Emerging roles of the nucleolus in regulating the DNA damage response: the noncanonical DNA repair enzyme APE1/Ref-1 as a paradigmatical example. Antioxidants. Redox. Signal. *20*, 621–639. https://doi.org/10.1089/ars.2013.5491.

20. Segales, J., Islam, A.B., Kumar, R., Liu, Q.C., Sousa-Victor, P., Dilworth, F.J., Ballestar, E., Perdiguero, E., and Munoz-Canoves, P. (2016). Chromatin-wide and transcriptome profiling integration uncovers p38alpha MAPK as a global regulator of skeletal muscle differentiation. Skeletal Muscle *6*, 1–15. https://doi.org/10.1186/s13395-016-0074-x.

21. Xu, J., Wang, K., Zhang, Z., Xue, D., Li, W., and Pan, Z. (2021). The Role of Forkhead Box Family in Bone Metabolism and Diseases. Front. Pharmacol. *12*, 772237. https://doi.org/10.3389/fphar.2021.772237.

22. Yin, H., Fan, X., Zhang, Y., Zhao, N., Zhao, X., Yin, K., and Zhang, Y. (2022). An Integrated Study on the Differential Expression of the FOX Gene Family in Cancer and Their Response to Chemotherapy Drugs. Genes *13*, 1754. https://doi.org/10.3390/genes13101754.

23. Golson, M.L., and Kaestner, K.H. (2016). Fox transcription factors: from development to disease. Development *143*, 4558–4570. https://doi.org/10.1242/dev.112672.

24. Katoh, M., Igarashi, M., Fukuda, H., Nakagama, H., and Katoh, M. (2013). Cancer genetics and genomics of human FOX family genes. Cancer. Lett. *328*, 198–206. https://doi.org/10.1016/j.canlet.2012.09.017.

25. Chen, Q., Zhuang, S., Hong, Y., Yang, L., Guo, P., Mo, P., Peng, K., Li, W., Xiao, N., and Yu, C. (2022). Demethylase JMJD2D induces PD-L1 expression to promote colorectal cancer immune escape by enhancing IFNGR1-STAT3-IRF1 signaling. Oncogene *41*, 1421–1433. https://doi.org/10.1038/s41388-021-02173-x.

26. Murtas, D., Maric, D., De Giorgi, V., Reinboth, J., Worschech, A., Fetsch, P., Filie, A., Ascierto, M.L., Bedognetti, D., Liu, Q., et al. (2013). IRF-1 responsiveness to IFN-gamma predicts different cancer immune phenotypes. Br. J. Cancer. *109*, 76–82. https://doi.org/10.1038/bjc.2013.335.

27. Wu, Y., Zhou, L., Zou, Y., Zhang, Y., Zhang, M., Xu, L., Zheng, L., He, W., Yu, K., Li, T., et al. (2023). Disrupting the phase separation of KAT8-IRF1 diminishes PD-L1 expression and promotes antitumor immunity. Nat. Can. (Ott.) *4*, 382–400. https://doi.org/10.1038/s43018-023-00522-1.

28. Ma, X., Jia, S., Wang, G., Liang, M., Guo, T., Du, H., Li, S., Li, X., Huangfu, L., Guo, J., et al. (2023). TRIM28 promotes the escape of gastric cancer cells from immune surveillance by increasing PD-L1 abundance. Signal Transduct. Targeted Ther. *8*, 246. https://doi.org/10.1038/s41392-023-01450-3.

29. Sharpe, A.H., and Pauken, K.E. (2018). The diverse functions of the PD1 inhibitory pathway. Nat. Rev. Immunol. *18*, 153–167. https://doi.org/10.1038/nri.2017.108.

30. Jiang, X., Wang, J., Deng, X., Xiong, F., Ge, J., Xiang, B., Wu, X., Ma, J., Zhou, M., Li, X., et al. (2019). Role of the tumor microenvironment in PD-L1/PD-1-mediated tumor immune escape. Mol. Cancer *18*, 10. https://doi.org/10.1186/s12943-018-0928-4.

31. Lee, J., Ahn, E., Kissick, H.T., and Ahmed, R. (2015). Reinvigorating Exhausted T Cells by Blockade of the PD-1 Pathway. Forum Immunopathol. Dis. Ther. *6*, 7–17. https://doi.org/10.1615/ForumImmunDisTher.2015014188.

32. Schneider-Poetsch, T., Ju, J., Eyler, D.E., Dang, Y., Bhat, S., Merrick, W.C., Green, R., Shen, B., and Liu, J.O. (2010). Inhibition of eukaryotic

translation elongation by cycloheximide and lactimidomycin. Nat. Chem. Biol. *6*, 209–217. https://doi.org/10.1038/nchembio.304.

33. Han, J., Perez, J.T., Chen, C., Li, Y., Benitez, A., Kandasamy, M., Lee, Y., Andrade, J., tenOever, B., and Manicassamy, B. (2018). Genome-wide CRISPR/Cas9 Screen Identifies Host Factors Essential for Influenza Virus Replication. Cell Rep. *23*, 596–607. https://doi.org/10.1016/j.celrep.2018.03.045.
34. Gou, Q., Dong, C., Xu, H., Khan, B., Jin, J., Liu, Q., Shi, J., and Hou, Y. (2020). PD-L1 degradation pathway and immunotherapy for cancer. Cell Death Dis. *11*, 955. https://doi.org/10.1038/s41419-020-03140-2.
35. Zhu, Q., Wang, H., Chai, S., Xu, L., Lin, B., Yi, W., and Wu, L. (2023). O-GlcNAcylation promotes tumor immune evasion by inhibiting PD-L1 lysosomal degradation. Proc. Natl. Acad. Sci. USA *120*, e2216796120. https://doi.org/10.1073/pnas.2216796120.
36. Huang, R., Wu, C., Wen, J., Yu, J., Zhu, H., Yu, J., and Zou, Z. (2022). DIAPH3 is a prognostic biomarker and inhibit colorectal cancer progression through maintaining EGFR degradation. Cancer Med. *11*, 4688–4702. https://doi.org/10.1002/cam4.4793.
37. Yamamoto, K., Venida, A., Yano, J., Biancur, D.E., Kakiuchi, M., Gupta, S., Sohn, A.S.W., Mukhopadhyay, S., Lin, E.Y., Parker, S.J., et al. (2020). Autophagy promotes immune evasion of pancreatic cancer by degrading MHC-I. Nature *581*, 100–105. https://doi.org/10.1038/s41586-020-2229-5.
38. Marks, M.S., Roche, P.A., van Donselaar, E., Woodruff, L., Peters, P.J., and Bonifacino, J.S. (1995). A lysosomal targeting signal in the cytoplasmic tail of the beta chain directs HLA-DM to MHC class II compartments. J. Cell. Biol. *131*, 351–369. https://doi.org/10.1083/jcb.131.2.351.
39. Almen, M.S., Nordstrom, K.J., Fredriksson, R., and Schioth, H.B. (2009). Mapping the human membrane proteome: a majority of the human membrane proteins can be classified according to function and evolutionary origin. BMC Biol. *7*, 50. https://doi.org/10.1186/1741-7007-7-50.
40. Fagerberg, L., Jonasson, K., von Heijne, G., Uhlén, M., and Berglund, L. (2010). Prediction of the human membrane proteome. Proteomics *10*, 1141–1149. https://doi.org/10.1002/pmic.200900258.
41. Muller, D.J., Wu, N., and Palczewski, K. (2008). Vertebrate membrane proteins: structure, function, and insights from biophysical approaches. Pharmacol. Rev. *60*, 43–78. https://doi.org/10.1124/pr.107.07111.
42. Cox, J.S., Shamu, C.E., and Walter, P. (1993). Transcriptional induction of genes encoding endoplasmic reticulum resident proteins requires a transmembrane protein kinase. Cell *73*, 1197–1206. https://doi.org/10.1016/0092-8674(93)90648-a.
43. Liao, Y., Goraya, M.U., Yuan, X., Zhang, B., Chiu, S.H., and Chen, J.L. (2019). Functional Involvement of Interferon-Inducible Transmembrane Proteins in Antiviral Immunity. Front. Microbiol. *10*, 1097. https://doi.org/10.3389/fmicb.2019.01097.
44. Mudumbi, K.C., Czapiewski, R., Ruba, A., Junod, S.L., Li, Y., Luo, W., Ngo, C., Ospina, V., Schirmer, E.C., and Yang, W. (2020). Nucleoplasmic signals promote directed transmembrane protein import simultaneously via multiple channels of nuclear pores. Nat. Commun. *11*, 2184. https://doi.org/10.1038/s41467-020-16033-x.
45. Lu, X., An, L., Fan, G., Zang, L., Huang, W., Li, J., Liu, J., Ge, W., Huang, Y., Xu, J., et al. (2022). EGFR signaling promotes nuclear translocation of plasma membrane protein TSPAN8 to enhance tumor progression via STAT3-mediated transcription. Cell Res. *32*, 359–374. https://doi.org/10.1038/s41422-022-00628-8.
46. Sardi, S.P., Murtie, J., Koirala, S., Patten, B.A., and Corfas, G. (2006). Presenilin-dependent ErbB4 nuclear signaling regulates the timing of astrogenesis in the developing brain. Cell *127*, 185–197. https://doi.org/10.1016/j.cell.2006.07.037.
47. Wang, S.C., and Hung, M.C. (2009). Nuclear translocation of the epidermal growth factor receptor family membrane tyrosine kinase receptors. Clin. Cancer. Res. *15*, 6484–6489. https://doi.org/10.1158/1078-0432.CCR-08-2813.
48. Aleksic, T., Gray, N., Wu, X., Rieunier, G., Osher, E., Mills, J., Verrill, C., Bryant, R.J., Han, C., Hutchinson, K., et al. (2018). Nuclear IGF1R Interacts with Regulatory Regions of Chromatin to Promote RNA Polymerase II Recruitment and Gene Expression Associated with Advanced Tumor Stage. Cancer. Res. *78*, 3497–3509. https://doi.org/10.1158/0008-5472.CAN-17-3498.
49. Huang, Y., Li, J., Du, W., Li, S., Li, Y., Qu, H., Xv, J., Yu, L., Zhu, R., and Wang, H. (2021). Nuclear translocation of the 4-pass transmembrane protein Tspan8. Cell Res. *31*, 1218–1221. https://doi.org/10.1038/s41422-021-00522-9.
50. Liu, Z., Yu, X., Xu, L., Li, Y., and Zeng, C. (2022). Current insight into the regulation of PD-L1 in cancer. Exp. Hematol. Oncol. *11*, 44. https://doi.org/10.1186/s40164-022-00297-8.
51. Rizzo, A., Santoni, M., Mollica, V., Ricci, A.D., Calabrò, C., Cusmai, A., Gadaleta-Caldarola, G., Palmiotti, G., and Massari, F. (2022). The Impact of Concomitant Proton Pump Inhibitors on Immunotherapy Efficacy among Patients with Urothelial Carcinoma: A Meta-Analysis. J. Personalized Med. *12*, 842. https://doi.org/10.3390/jpm12050842.
52. Pan, S., Shen, M., Zhou, M., Shi, X., He, R., Yin, T., Wang, M., Guo, X., and Qin, R. (2019). Long noncoding RNA LINC01111 suppresses pancreatic cancer aggressiveness by regulating DUSP1 expression via microRNA-3924. Cell Death Dis. *10*, 883. https://doi.org/10.1038/s41419-019-2123-y.
53. Li, J., Wang, Y., Wang, L., Hao, D., Li, P., Su, M., Zhao, Z., Liu, T., Tai, L., Lu, J., and Di, L.J. (2023). Metabolic modulation of CtBP dimeric status impacts the repression of DNA damage repair genes and the platinum sensitivity of ovarian cancer. Int. J. Biol. Sci. *19*, 2081–2096. https://doi.org/10.7150/ijbs.80952.

STAR★METHODS

KEY RESOURCES TABLE

REAGENT or RESOURCE	SOURCE	IDENTIFIER
Antibodies		
Anti-TMEM199	Boster, China	Cat # A14686-1
Anti-Flag	Sigma	Cat#F1804
Anti-PD-L1	R&D	Cat#1019
Chemicals, peptides, and recombinant proteins		
RIPA Buffer	Thermo	Cat# 89901
protease inhibitor	Sigma	Cat#SRE0055
Experimental models: Cell lines		
HEK293T	ATCC	
143B	ATCC	
CAOV3	University of Macau	
Oligonucleotides		
Target: mouse TMEM199#1, 5′-3’: TTGCTTGCCGGCGAACGAC; 3′-5’: GTCGTTCGCCGGCAAGCAA. Target: mouse TMEM199#2, 5′-3’: TTCGCGCTTTGGGTCCTGG; 3′-5’: CCAGGACCCAAAGCGCGAA. Target: mouse TMEM199#3, 5′-3’: AGCCAATGAGGAGTATAAG; 3′-5’: CTTATACTCCTCATTGGCT. Target: mouse TMEM199#4, 5′-3’: GAGCTGGGCACGCAGCTTC; 3′-5’: GAAGCTGCGTGCCCAGCTC. Target: human TMEM199#1, 5′-3’: GTGCAGATCCCGGATGAGA; 3′-5’: TCTCATCCGGGATCTGCAC. Target: human TMEM199#2, 5′-3’: AAGCTCGGCCCGCAGCTTT; 3′-5’: AAAGCTGCGGGCCGAGCTT. Target: human TMEM199#3, 5′-3’: CCAGAACTAGTTGCCCGGC; 3′-5’: GCCGGGCAACTAGTTCTGG. Target: human TMEM199#4, 5′-3’: GGTGGGACTCTCAGCGACC; 3′-5’: GGTCGCTGAGAGTCCCACC.		
Software and algorithms		
R software		

EXPERIMENTAL MODEL AND STUDY PARTICIPANT DETAILS

Cells

HEK293 cells, 143B cells, and CAOV3 cells were all maintained in regular DMEM supplemented with 10% (v/v) FBS, penicillin–streptomycin. All the cells were identified by STR. Cells were professionally certified and tested for mycoplasma contamination.

Mice

Male BALB/c mice (6–8 weeks old) (Pengyue Laboratory, Jinan, China) were subcutaneously injected with 1×10^5 4T1 cells (labeled by luciferase expression cassette, Addgene 72485) in each hindlimb and randomly divided into different experimental groups 5 weeks after cancer cells injection. The Tumors were surgically removed after various administrations for further estimation. Mice experiments were approved by the Animal Research Ethics Committee of Weifang Medical University (2022SDL065). All procedures were performed with relevant guidelines and laws.

METHOD DETAILS

Cell lines, chemicals and antibodies

HEK293 cells, 143B cells, and CAOV3 cells were all maintained in regular DMEM supplemented with 10% (v/v) FBS, penicillin–streptomycin. The antibodies applied in this study include Anti-Transmembrane Protein 199 TMEM199 Antibody (Boster, A14686),

anti-Flag antibody (Sigma, F1804), anti-Tubulin antibody (Beyotime, AF1216), anti-CD274 (Biolegend, 329706) and anti-CD8α (Biolegend, 100708). The chemicals include IFNγ (Biolegend, 505832), CCK8 Kit (Beyotime, C0038), Vectors and oligos.

For mammalian expression plasmids, full TMEM199 sequences were amplified and assembled into the expression vectors with Flags or eGFP. Trucked TMEM199 sequences were amplified and assembled into the expression vectors with Flags. The sequences were assembled into a modified pSIN vector (Addgene,16578) with a one-step cloning kit (Vazyme, C113-02). HEK293T cells were used to package the lentivirus, and the supernatant was harvested post-transfection for 72 h, and spun down, filtered with a 0.45μM syringe filter. The target cells were infected and further selected with Puromycin (2ug/ml) for stable cell lines.

CCK8 assay

143B or HCT116 cells were seeded into 96-well plates with 2,500 cells per well, then cultured in the full DMEM medium for indicated time courses. Afterward, CCK8 was added into the medium for 1 h as per the instructions of the Kit protocol. The cell viability can be simply estimated by recording the optical density (OD) of formazan at 450 nm using a plate reader (PerkinElmer VictorX3).

Transwell migration assay

Cells (5 × 104 cells per well) were seeded in the top chambers of the transwell plates in FBS-free media with membrane inserts. 0.6mL DMEM supplemented with 10% FBS was added to the well of the plate (lower compartment). The cells were incubated in the plate for 48h. Then stained with crystal violet and photographed by microscopy.

Co-IP assay

Cytoplasmic and nuclear protein fractionation and isolation were performed using the Protein Extraction Kit (Boster Biological Technology) in consonance with the manufacturer's introductions as prescribed previously.[52] IP buffer is constituted of 20 mM Tris-HCl, pH 8.0, 100 mM NaCl, 1 mM EDTA, 0.5%NP-40) containing 50 mM β-glycerophosphate, 10 mM NaF, 1X Proteinase inhibitor, and 1XPhosphatase Inhibitor. The cell lysate was sonicated for 10 cycles with 30 s' on and 30 s' off using a sonicator (Qsonica Q700). The Supernatant after centrifugation at 12500 rpm for 10min was used as input. Then, cell lysates were incubated with 1μg of antibody and Protein G and A Dynabeads (Thermo Fisher) overnight at 4°C. The immunocomplexes pulled down were further used for immunoblotting detection or MS analysis.

Protein identification by MS and bioinformatic analysis

LC-MS detection was executed by Applied Protein Technology (Shanghai, China). 5800 MALDI-TOF/TOF (AB Sciex, USA) was used for mass spectrometer (MS) data analyses. Bioinformatic analysis was done by R software.

Colony formation assay

1000 Cells were plated in triplicate in each well of 6 well plates. Cells were cultured for 14 days at 37°C to allow colony formation. Colonies were stained with 5% GIEMSA and counted.

Immunofluorescence assay

The immunofluorescence assay was performed as described previously.[53] Briefly, Cells were grown on coverslips. The cells were washed twice with PBS and fixed in 3.5% paraformaldehyde. After washing the fixed cells with PBS 3 times, the cells are permeabilized in PBS supplemented with 10% goat serum and 0.3% Triton X-100 for 15mins. Then the cells were treated with 3% H2O2 for 10mins and washed twice. The cells were treated by blocking buffer (10% goat serum in 1xPBS) for 1h. The cells were incubated with primary antibody (1:50 for anti-TMEM199 antibody, 1:100 for anti-Flag antibody) in a blocking buffer for 1.5h. After washing, the cells were incubated with Alexa Fluor 488 Goat Anti-Mouse IgG for 1h. After washing the cells 3 times in PBS, the coverslips were mounted using VECTASHIELD with DAPI.

Western blotting

The cells were lysed on ice using RIPA Buffer (Thermo # 89901) with the presence of a cocktail protease inhibitor (Sigma #SRE0055). The total protein (~20 μg) from each sample was separated by SDS-PAGE in SDS running buffer (TAKARA #T9101) at 150 V for 1h at room temperature and transferred to PVDF membranes at 300mA for 3h at 4°C. Blots were then probed with primary antibody at 1:1000 overnight at 4°C. Then the membrane was washed and incubated with HRP-conjugated secondary antibody (Santa Cruz) at 1:5000 dilution. After being washed 5 times in PBST, the membrane was incubated with ECL detection reagent (#RPN2235) and then visualized with ChemiDoc Touch Imaging system (Bio-Rad).

Transcriptome analysis

Total RNA was extracted from cells using TRIzol. After library construction, RNA sequencing was performed using an Illumina sequencer with a 150 bp paired-end sequencing reaction. Raw FASTQ files were trimmed by FASTp (v0.23.2). Adapters were removed and low-quality reads were filtered out. Then, Data was mapped to hg19 with Tophat2, and gene expression FPKM was obtained with Cufflinks. Default parameters were used for these tools. Differentially expressed genes were defined as genes with 1.0-fold-change differences. The functional enrichment analysis was done with cluster Profiler.

Cut&Tag assay

Cut&Tag assay was performed as described (37052060). A CUT&Tag library was constructed using Hyperactive Universal CUT&Tag Assay Kit for Illumina (Vazyme, TD903). Briefly, Concanavalin A-coated magnetic beads were rinsed in the binding buffer while cells were collected, counted, and rinsed in the wash buffer. After immobilization of the cells on the beads, buffer containing digitonin antibody was used for permeabilization, with consequent incubating with primary antibodies for Anti-TMEM199 (1:50) overnight at 4°C. Consequently, cultures were rinsed/exposed to a second antibody (60 min/RT). Preparation of the pA-Tn5-adapter transposons involved three washes (1h for each) of the pA-Tn5 complex with Dig300 buffer. The pA-Tn5 was then incubated with the cells in a tag mentation buffer (60 min/37C). After stopping the tag mentation process, the DNA was solubilized by the addition of EDTA, SDS, together with proteinase K, with consequent extraction via phenol/chloroform/ethanol-precipitation. DNA was finally amplified by PCR for insertion of the next-generation sequencing indices and purified before sequencing the CUT&Tag libraries. CUT&Tag raw files were quality controlled with FastQC v0.11.3, and human CUT&Tag reads were individually aligned to the human genome construct GRCh38 using bowtie2 v2.4.2 software.24 Genome browsing tracks for the UCSC Genome Browser were created using deepTools bam Coverage v3.5.1 (-normalize Using Reads Per Kilobase Million [RPKM]). CUT&Tag peak distribution created using deep Tools computeMatrix and plotHeatmap.

Animal experiment

All the animal experiments were approved by the Animal Research Ethics Committee of Weifang Medical University (2022SDL065). Male BALB/c mice (6–8 weeks old) were subcutaneously injected with 1×10^5 4T1 cells (labeled by luciferase expression cassette, Addgene 72485) in each hindlimb and randomly divided into different experimental groups 5 weeks after cancer cells injection. The Tumors were surgically removed after various administrations for further estimation.

QUANTIFICATION AND STATISTICAL ANALYSIS

Statistical analysis was performed using Student's t-test except specific marked and expressed as median with Standard deviation. $p < 0.05$ was considered significant. The symbol * indicates $p < 0.05$; ** indicates $p < 0.01$; ***indicates $p < 0.001$.